Journal of Thermal Analysis and Calorimetry (2024) 149:11577–11586
https://doi.org/10.1007/s10973-024-13564-z

# The efficiency assessment of $Ni_{(40)}Ti_{(50)}Cu_{(x)}Fe_{(10-x)}$ shape memory alloy produced by combustion synthesis through thermal analysis

**Berk Keskin**[1] · **Bora Derin**[2]

Received: 8 October 2023 / Accepted: 3 August 2024 / Published online: 7 October 2024


**Abstract**
In this investigation, $Ni_{(40)}Ti_{(50)}Cu_{(x)}Fe_{(10-x)}$ ($x = 2.5, 5, 7.5$) alloys were synthesized through the self-propagating high-temperature synthesis (SHS) process, employing preheating temperatures of 240 and 450 °C. To optimize thermal analysis, samples were drawn from the middle and upper sections of specimens exhibiting superior propagation results at a preheating temperature of 450 °C. Omitting additional heat treatment ensured a precise result interpretation. While the $Ti_{50}Ni_{40}Fe_{2.5}Cu_{7.5}$ sample displayed minimal variations in martensite and austenite transformation temperatures, others exhibited diverse transformation profiles. Apart from the B19' martensitic phase, distinct B19 martensitic phases were identified in $Ti_{50}Ni_{40}Fe_5Cu_5$ and $Ti_{50}Ni_{40}Fe_{2.5}Cu_{7.5}$ alloys, each showcasing unique transformation temperatures and full-width at half-maximum (FWHM) values. The inquiry unveiled that an increased Fe content prompted the segregation of $Fe_x$(Ni)Ti-based intermetallic phases from Cu-based phases, with this effect intensifying in alloys featuring higher Fe atomic ratios. This influence significantly impacted transformation temperature outcomes, overshadowing the inherent impact of the synthesis method.

**Keywords** SHS · NiTiCuFe · Thermal analysis · Factsage · Shape–memory alloys

## Introduction

NiTi is a well-known shape memory alloy that finds extensive applications in various fields, particularly in the biomedical industry and as an actuator. It is highly regarded for its biocompatibility with human tissue, resistance to corrosion, nonmagnetic properties, and mechanical similarity to the human skeleton [1].

Modifying the NiTi intermetallic by adding third alloy elements can have a significant impact on the transformation temperature and hysteresis characteristics. Previous studies have demonstrated that the substitution of Fe atoms in the Ni site of the NiTi structure leads to a decrease in transformation temperatures. Choi et al. synthesized the (50-$x$)-Fe($x$) intermetallic compound using an arc melter system with a molar ratio range of $2 < x < 20$. It was observed that Fe content above 6 at.% stabilizes the austenite phase and inhibits the formation of the martensitic structure. On the other hand, the addition of Cu increases the initial temperature of the B19 (orthorhombic) martensitic phase (Ms.) and decreases the initial temperature of the B19' (monoclinic) martensitic phase. In other words, the dominance of the B19 phase over B19' increases with higher Cu ratios, while the Ms. temperature of B19' decreases. B19' is effectively suppressed when the Cu at.% ratio exceeds 20 at.%. Furthermore, an increase in Cu ratio brings the transformation intervals of As-Af and Ms-Mf closer together [2–4]. Although this sensitivity to transformation allows NiTiCu to be utilized as an actuator, the presence of copper above 12.5 at.% makes shaping the material difficult and may lead to breakage during hot rolling. [5, 6] Some researchers have proposed alloying the material with a 4th element such as Nb to prevent this phenomenon [7]. Lo et al. investigated the phase transformations of B19 and B19' through dynamic XRD analysis on samples alloyed with 10 at.% Cu. Numerous studies in the literature have focused on the phase transformations in NiTiCu alloys. [4, 8, 9].

Limited research has been conducted on quaternary alloys containing Fe and Cu. In these studies, only the ratio of

✉ Berk Keskin
bkeskin@medipol.edu.tr

[1] Construction Technology Department, Istanbul Medipol University, Kavacık, North Campus, Room:337, Istanbul, Turkey

[2] Metallurgical and Materials Engineering Department, Chemical and Metallurgy Faculty, Istanbul Technical University, Maslak, Istanbul, Turkey

the added fourth element varies. For instance, Tong et al. investigated the cycling stability of martensitic transformation in $(Ti_{54}Ni_{34}Cu_{12})_{100-x}Nb_x$ alloy. It was observed that with increasing Nb content, the Ms and As transformations remained within the range of 0.1–0.3 °C, respectively [10]. Lai et al. studied the $Ti_{50-x}Ni_{48}Fe_2Nb_x$ alloy and found that increasing Nb content (from 0.5 to 2 at.%) suppressed the R phase and led to a decrease in Ms temperature [11]. Chluba et al. fabricated the $(Ti_{55}N_{i33}Cu_{12})_{100-x}Fe_x$ alloy using thin film technique and observed a decrease in Ap and Mp values with increasing Fe content (ranging from 0.7 to 1.6 at.%) [12]. In addition to these, several studies have been conducted on NiTiFeCu as a high-entropy alloy, and in these studies, their microstructures and mechanical properties have also been discussed [13, 14].

While the effects of triple alloy elements in NiTi have been extensively studied in the literature, the impact of a fourth element, such as Cu and Fe, remains relatively unexplored. Additionally, many studies have been conducted using vacuum-arc and vacuum induction methods; however, in this study, the self-propagating high-temperature synthesis (SHS) method will be utilized. The stoichiometric atomic ratios of Ni and Fe/Cu elements varied while keeping the Ti content constant. The primary goal is to investigate how the segregation of solid solutions (or intermetallic compounds) affects the transformation temperature, given that Cu and Fe have different affinities for Ni and Ti. The reaction does not reach equilibrium due to the SHS method. There is very limited solid-state diffusion, so the segregation of these compounds is examined to understand how it influences the transformation temperature in different parts of the material. As a result, the microstructures of the produced alloys were investigated using electron microscopy and X-ray diffraction techniques. Samples taken from the upper and middle levels of the specimen were examined using thermal analysis techniques.

## Experimental

In the experiments, $Fe_xCu_{(10-x)}$ ($x = 2.5$, 5, 7.5 at.%) powders were combined with a mixture of $Ni_{40} + Ti_{50}$ (at.%) powders, and two distinct preheating temperatures were utilized. The brand of powders used in the experiments is Alfa Aesar, and the properties are as follows: Ni (3–7 $\mu m$ dendritic, > 99.9%), Ti < 106 $\mu m$, spherical, > 99.9%), Fe and Cu (10 $\mu m$, spherical, > 99.9%).

The mixture was homogenized for 15 h in a tubular mixer without any additives. Subsequently, a hard pellet, resembling the sample depicted in Fig. 1, was obtained by applying a pressure of approximately 65 MPa using a hydraulic press in all experiments. The post-press diameters and lengths of the samples were measured as 12.5 and approximately

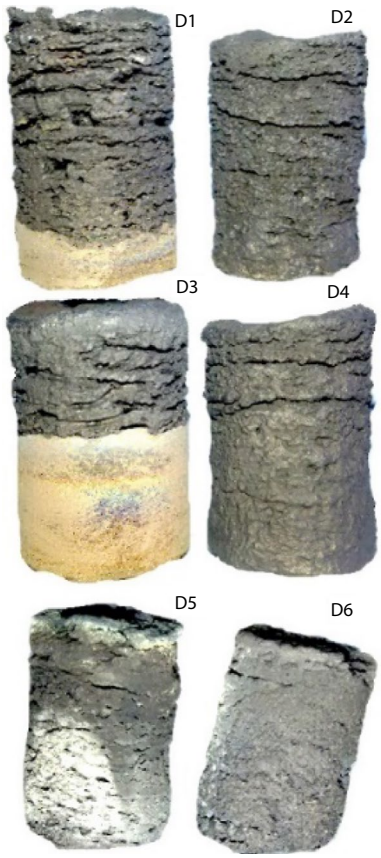


**Fig. 1** Macrostructures of the synthesized samples

19.5 mm, respectively. The NiTiFeCu shape memory alloy (SMA) was synthesized through the self-propagating high-temperature synthesis (SHS) technique using a specially designed valve reactor. Throughout the entire experimental procedure, a high-purity argon atmosphere was maintained. The atmosphere was evacuated twice using a vacuum pump to reduce it to $10^{-3}$ mbar before being refilled with high-purity argon gas to attain room pressure.

The reactor employed two independently controlled variacs to regulate preheating and initiating the combustion reaction. Additionally, two thermocouples were placed inside the reactor to measure temperature changes, while the temperature profile was recorded by a computer. The combustion waves were captured by an HD camera for subsequent analysis after the propagation process was completed (see supplementary files for the propagation videos). In each experiment, a consistent ignition wire geometry was employed, which comprised 20 windings with a diameter of 2.5 mm and a total length of 28 cm. It was positioned 3–7 mm away from and parallel to the sample, providing similar power levels ranging from 650 to 700 W. No heat treatment (aging or homogenization) was performed after synthesizing the samples.

In this study, the phases formed in the microstructure were analyzed using a Bruker™ D8 XRD device, phase transformations were investigated using a Seiko 220 C DSC device. The heating rate was 10 K $min^{-1}$., followed by two cycles. The morphology of selected samples was examined using a Hitachi SU70 FE SEM–EDS instrument. Lastly, a solution composed of $HF + HNO_3 + H_2O$ was utilized to etch the sample for microstructure investigation, followed by optical microscopy.

## Heating regime and ignition temperature values

The porosities on the outer surface are more interconnected and noticeable at lower preheating temperatures, while the formations appear more compacted at higher preheating temperatures. Additionally, the top surface exhibits more slits than the lower sections due to increased heat resistance (see Fig. 1).

The heating regimes of samples were depicted in Fig. 2 and Table 1. Additionally, the propagation behavior could be explored in the supplementary files through videos. Samples D1, D3, D5 were preheated to a temperature of 230/240 °C at rates of 18.8 °C mins.$^{-1}$, 17.9 °C mins.$^{-1}$, 18.5 °C mins.$^{-1}$, respectively, and ignition was achieved by applying current to the W wire for various times with the same power. For samples D5 and D6 (5 Cu, 5 Fe at.%), the maximum combustion temperatures were not measurable and were indicated with a cross symbol (×) in Fig. 2. During the synthesis, it has been observed that not only the propagation times but also the ignition times are of significance. The reactions for samples D3, D5, and D1, synthesized at a preheating temperature of 230/240 °C, initiated after 9.1, 1 and 2 s. respectively. Particularly, in the case of sample D3 with a high copper content (240 °C preheating temperature), although ignition persisted for 59 s, propagation could not be completed. However, due to the substantial heat it received, 47% of its length progressed rapidly within 3.86 s. Sample D5, which received energy through ignition wire for approximately 2 s longer than D1, was completed 100%, yet the completion times for both samples were approximately 15 s. The rate of propagation of samples D3 (7.5 at.% Cu), D5 (5 at.% Cu), and D1 (2.5 at.% Cu) were found to be 2.37 mm $s^{-1}$, 1.56 mm $s^{-1}$, and 1.52 mm $s^{-1}$, respectively. While D3 may appear to propagate faster, it did so in an unsteady regime, with the propagation resembling volume combustion due to the heat-affected zone caused by the ignited wire. D5, on the other hand, paused for about 3.2 seconds near the middle region before propagating In contrast, D1 exhibit steady-state propagation, leading to more reliable results. In summary, it can be concluded that an increased copper content hinders the reaction, and a preheating temperature of 240 °C is relatively low for propagation. This can be elucidated by considering the mixing enthalpy of the binary elements as listed in Tables 2 and 3. The positive mixing enthalpy observed in the Cu-based alloys reduces the driving force for propagation.

In Fig. 2, as expected, the maximum temperatures reached in samples produced at a preheating temperature of 450/455 °C were higher. Samples D4, D2, D6 were heated at speeds of 21.4 °C mins.$^{-1}$, 19.4 °C mins.$^{-1}$, 18.5 °C mins.$^{-1}$, respectively, and it was observed that the reaction started by keeping the W wire open for 4 s. The propagation was completed to the end for these samples between 2 and 2.9 s. Due to their high liquefaction, these samples exhibited a

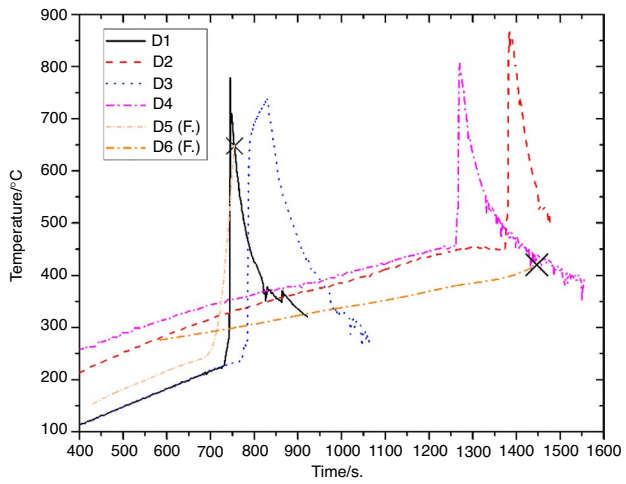


**Fig. 2** Heating regime of the samples

**Table 1** Various properties in the synthesis of the samples (*:It paused for given time near the middle part, then propagated.)

| Composition (at.%) Ti: 50 at.% Ni: 40 at.% | Short name | Total ignited time of the samples / (s.) | Propagation time / (s.) | Starting time of the propagation process following ignition / (s.) |
|---|---|---|---|---|
| 7.5Fe–2.5Cu | D1 | 8.86 | 12.8+1* (~85%) | 2.01 |
| 7.5Fe–2.5Cu | D2 | 6.18 | 2.9 | 4.05 |
| 7.5Cu–2.5Fe | D3 | 59 | 3.86 (~47%) | 9.17 |
| 7.5Cu–2.5Fe | D4 | 5.06 | 1.94 | 3.17 |
| 5Cu–5Fe | D5 | 10.8 | 12.5+3.2* (100%) | 1 |
| 5Cu–5Fe | D6 | 3 | 2.31 | 1.88 |

more compact structure and collapse. The propagation time results were very close to each other around 2 s. The fluctuation (1.9 to 2.9 s.) was probably due to uncontrollable power surges caused by the variac. It can easily be said that preheating temperature about 450–455 is enough to ignite all these samples without completely melting.

## Thermodynamic investigation

Factsage 7.1 Thermochemical Computer-Based Software (with SGTE 2014 database) was used to investigate the thermodynamic properties of the selected alloys. The alloy was treated as a high-entropy alloy (HEA), allowing for a clear understanding of the segregation of solid solutions and intermetallic compounds. Zhang et al. showed that δ (atomic-size difference in multicomponent alloys), values of mixing entropy and mixing enthalpy are important parameter for specifying the crystal structure of alloy (BCC, B2, FCC) [15]. Yang et al. showed $\Omega(=Tm.\Delta Smix.\Delta Hmix^{-1}$, where Tm: The average Tm of the element with the respective ratio) > 1 for disordered system while ΔHmix < -15 kJ. $mole^{-1}$ for ordered intermetallic system [16]. Singh et al. showed that $\Lambda(=\Delta Smix.\delta^{-2}) < 0.25$ and 6.6% < δ for ordered system that related with atomic mismatch leads to local elastic strain [17]. If δ is high, the likelihood of laves phases occurring is increased [15]. Values of these parameters are calculated for NiTi, NiTiFeCu and present alloys. ΔHmix was calculated with help of Factsage Thermochemical Software and studies of Takeuchi et al. [18] based on Miedema et al. [19]. It was presented in Tables 2 and 3.

The produced samples' mixture enthalpy and entropy values appear to be closer to the NiTi intermetallic rather than the high-entropy alloy NiTiCuFe. This implies that the conditions for ΔHmix, ΔSmix, Λ, δ, and Ω are met for the intermetallic product. The values of Ω and ΔSmix for NiTiFeCu7.5 and NiTiFeCu2.5 products are intermediate between NiTiFeCu and NiTi. The ΔHmix value of the NiTi phase is negative at −38 $kJ.mol^{-1}$, generating exothermic energy and leading to intermetallic structure formation. The NiTiFeCu2.5 alloy (−32.2 $kJ.mol^{-1}$) is more negative than NiTiFeCu7.5 (−30.2 $kJ.mol^{-1}$), indicating higher exothermic energy. Moreover, the Fe–Ti mixture enthalpy value is the most negative after the Ni–Ti mixture enthalpy value, suggesting the likelihood of structural segregation. Both quaternary and binary ΔHmix values support this scenario. Figure 3 represents the temperature graph of the standard Gibbs free energy for binary systems with negative values, which indicates the likelihood of forming intermetallic compounds. Among these, Ni–Ti intermetallic is considered the most stable, followed by FeTi, CuTi, and NiFe compounds. In summary, considering kinetic factors, the probability of separation of NiTi and FeTi from CuTi and NiFe intermetallics is high.

Upon examining the products of combustion synthesis, the sample contained a high Cu content of 7.5 propagates halfway despite being exposed to triggering at lower temperatures for a longer period. Considering that even NiTi struggles to propagate despite having a more negative mixture enthalpy at 200 °C preheating, this situation becomes understandable [20].

# Results

## XRD analysis

The samples that were synthesized at 450 °C were selected for metallographic, thermal and XRD analysis. D2-D4-D6 samples were chosen for XRD analysis because these were propagated completely. For simplicity, the samples were

**Table 2** Mixing enthalpy of binary system

| | Fe–Ti | Ni–Ti | Cu–Ti | Ni–Cu | Cu–Fe | Ni–Fe |
|---|---|---|---|---|---|---|
| Mixing Enthalpies ($kJ.mol^{-1}$) | −17 (*M) | −35 (*M) | −9 (*M) | 4 (*M) | 13 (*M) | −2 (*M) |

*M: Miedema model

**Table 3** Various thermodynamic calculations were performed on both the NiTi and $NiTiFe_xCu_y$ phases

| | δ (×100) | ΔSmix / ($J.K^{-1}.mol^{-1}$) | ΔHmix / ( for 1500 °C, $kJ.mol^{-1}$) | Λ ($\Delta Smix/\delta^2$) | Omega |
|---|---|---|---|---|---|
| NiTi | 7.9764 | 5.76 | −38 | 0.119428408 | 0.27 |
| $Ni_{40}Ti_{50}Fe_{2.5}Cu_{7.5}$ | 7.8186 | 8.31 | −30.2 | 0.135938632 | 0.49 |
| $Ni_{40}Ti_{50}Fe_{7.5}Cu_{2.5}$ | 7.9518 | 8.31 | −32.2 | 0.131423155 | 0.47 |
| $Ni_{40}Ti_{50}Fe_5Cu_5$ | 7.8857 | 8.42 | −31.2 | 0.135388634 | 0,49 |
| NiTiCuFe | 6.9448 | 11.5 | −14.4 | 0.180753892 | 1.36 |

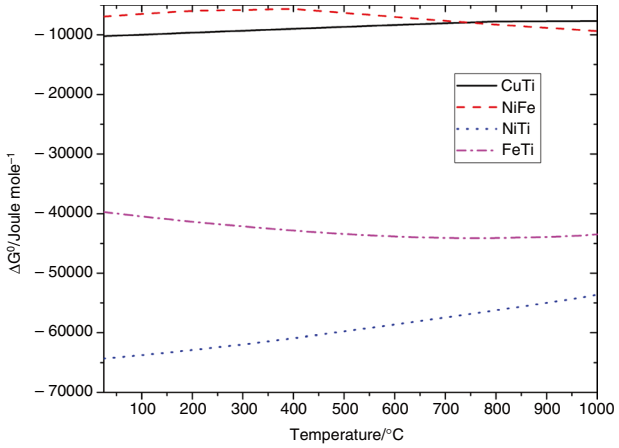


**Fig. 3** Standard Gibbs free energy versus temperature of the products

assigned the following codes: Cu2.5, Cu7.5, Cu5; D2, D4, and D6, respectively. In Fig. 4, B2 and $Ti_2Ni$ phase (mixed with $Ti_4Ni_2O_1$) were found in the all sample. Small amount retained B19' phases were found in 39°, 44°, and 44.81° [5]. There was no clear clue for R phase, but B19 was found in Cu7.5 and Cu5 in the XRD analysis at 40°. The R phase may be overlapping with the main peaks. The mixture of TiFe–TiFeNi phases was discovered behind the main B2 phase.

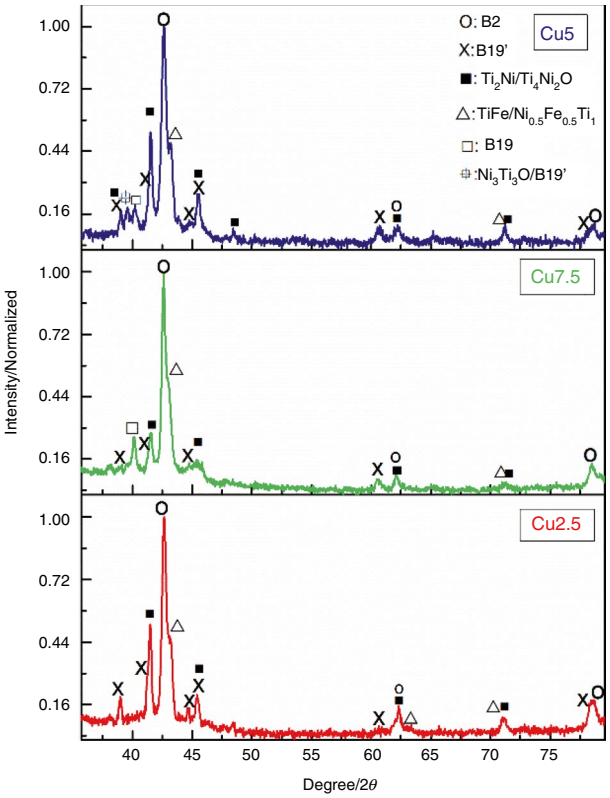


**Fig. 4** XRD values of the sample D2(Cu2.5), D4(Cu7.5), and D6(Cu5)

## Optical and SEM analysis

Figure 5 shows the optical analysis conducted on samples labeled Cu2.5, Cu5, and Cu7.5. The images revealed prominent large and circular black areas, which indicated gaps formed during the reaction. Subsequently, these gaps were filled with resin during the molding process. A near-dendritic network structure was predominantly observed in Cu2.5 samples, surrounding the microstructure to varying extents. This structure was postulated to consist of various intermetallic phases, a blend of Ti–Ni–Fe, later confirmed through SEM–EDS analysis. An increase in the Fe ratio led to the presence of more dendritic regions, while the addition of Cu resulted in a more equiaxed structure. In Cu5 samples, the grains were easily distinguishable, transforming into a cauliflower-like microstructure that falls between dendritic and cellular types. Interestingly, regions rich in Fe and Cu appeared to be somewhat segregated from each other, potentially hindering dendritic structure formation. Additionally, Cu-rich clustered regions were observed.

EDS analysis was conducted on samples D2 (Cu2.5) and D4 (Cu7.5) using low magnifications (500 × 500 µm and 1000 × 400 µm). In D2, Ti and Ni were found to be present at approximately 51.7.5–52.6 at.% and 37.5–39 at.%, respectively. However, it was observed that the distribution of Cu and Fe in sample Cu2.5 was not uniform. The elemental mapping revealed regions with $TiNiFe_xCu_y$ (with $5.85 < x < 8$ at.%) and ($0 < y < 2.68$ at.%), indicating the absence of Cu in certain regions and the presence of Fe-enriched microstructures (as shown in Fig. 6b). Further investigation at a magnification of × 1000 revealed that the dark dendritic regions consisted of $Ti_2Ni$ with embedded Fe elements, while Cu was predominantly present in the main phase, appearing as white regions. Regarding the primary phase, Cu was found to be present in accordance with the expected ratio, while Fe was generally detected within the structure in the range of 5 to 12 at.% (as shown in Fig. 6a). Besides the principal phase, which exhibited a lighter color, $Ti_2Ni$(Fe) intermetallics formed a dendritic network surrounding the structure, consistent with observations made using optical (light) microscopy. It is worth noting that the dark phase contained approximately 1.5 at.% Fe and lacked Cu. In certain regions, particularly highlighted in Fig. 6b, very dark agglomerations were evident. These regions were notably rich in Fe, constituting approximately 16 at.%, and did not contain Cu.

In the Cu7.5 sample, the Fe content was lower, and a more homogeneous distribution was observed ($TiNiFe_xCu_y$ ($1.87 < x < 3.81$ at.%) and ($6.63 < y < 7$ at.%)). However, the dark regions were significantly enriched in iron ($17 < x < 22$

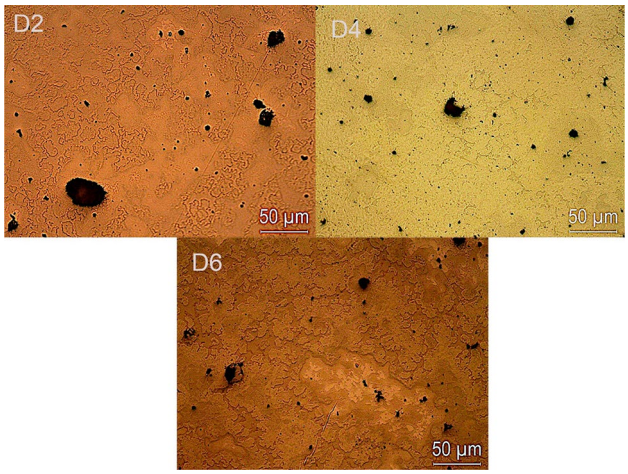


**Fig. 5** Optical images of sample D2, D4, and D6

at.%). Occasionally, the main phase contains a lower Fe atomic ratio. This observed difference in distribution could be attributed to the negative mixing enthalpy of Fe(Ni)–Ti intermetallics and the positive mixing enthalpy of Cu with the relevant elements, resulting in phase separations.

## DSC analysis

Past studies for comparison are presented in Table 4. Except for the samples by Moore et al., (by SHS) the other specimens [21] were fabricated using induction or arc or arc melting, followed by a high-temperature homogenization heat treatment [2, 4, 22]. This procedure clarifies the distinct differences among methods in terms of phase transformation temperatures or the more distinct emergence of phases like R and B19'. Considering this observation, based on the metallographic analysis and due to the nature of the SHS, the measurements were made from 2 different parts. Test pieces were taken from the upper and the middle part of the samples.

Figure 7 shows transformation temperatures of the samples. As and Mf were clearly not specified for all samples; however, considering the values of Ap and Mp provided greater reliability. Since the transformations of As-Af and Ms-Mf took place in a wide range for Cu2.5, the B2- > B19 transformation was observed in Cu7.5. Additionally, a slight occurrence of possible B19- > B19' transformation was detected at lower temperatures (Ap: 0, Mp: −22 °C). Nam et al. noted that detecting the B19- > B19' transformation with DSC was challenging because it was very diffusive, and B19 is a twinless, defect-free martensite; hence, the transformation was only observed in the upper section [2]. Additionally, the transformation enthalpy was quite low. In Cu5 (both mid. and up. section), two martensitic transformations with high enthalpies were observed. Since $\Delta H_{(B2<->B19')} > \Delta H_{(B2<->B19)} > \Delta H_{(B19<->B19')}$, the B19- > B19' transformation had a lower transformation enthalpy value; during cooling, it was inferred that the sequence was B2- > B19 and then B2- > B19'. The XRD results also supported this observation. Similar findings were reported by Valeanu et al. [23].

The Ms temperatures of the middle and upper parts of the Cu2.5 sample were 2 °C and 18 °C, respectively. These temperatures might potentially have been linked to the R martensite and therefore referred to as M1. There is no clear clue in the XRD analysis indicating the presence of B19 or R phase. Additionally, an unclear and broad intermediate martensite phase transformation was observed in the Cu2.5 sample (Ap: 75, Mp: 50 °C, named M2). It could have been related to another B19' or R peak due to the inhomogeneities such as NiTiFe and NiTiCu. These phases reduced Cu or Fe ratio in the B2 phase, thus causing splitting [9, 24] in the main peak due to the precipitates, or in the grain, and nano-crystallites may have transformed to the martensite phase simultaneously [25]. According to previous studies in the literature, the change in the Cu at.% rate does not make a significant difference in Ms [2, 4]. However, it was observed that the transformation temperatures decreased with an increase in Fe content in Table 5. Contrary to the literature, martensitic transformation was observed even at 7.5 at.% of Fe. It can be said that Cu had a more dominant role in transformation temperatures and phase transitions compared to Fe.

Maximum peak points for middle samples shifted to lower temperatures, and the values of the Af-Ms (or Ap-Mp) increased with increasing Fe atomic ratio (Cu2.5 < Cu5 < Cu7.5). Only Cu2.5 (mid) did not conform to this observation. This could be due to inhomogeneity. It can be said that iron had two roles here: the first was to reduce the temperature of Ms, and the second was to stabilize the R phase because Fe created more distortion in the structure compared to Cu. It hindered the transformation, leading to increased stability of the B2 phase. Particularly, the δ value increased with the addition of Fe. Zhang et al. explained this as the result of Fe's antisite behavior in the B2 phase [26]. Also, the ratio of Ni increased behind the ratio of Ti decreased. Several studies have shown that even a 1 at.% increase in nickel molar ratio dramatically decreased Ms [5, 26, 27].

## Discussion

The samples produced by SHS were found to yield nearly homogeneous products unless segregation occurs due to differences in atomic masses during the mixing process prior to synthesis. The critical parameter is the correct selection of the preheating temperature; otherwise, propagation will not be completed due to the weak exothermic energy

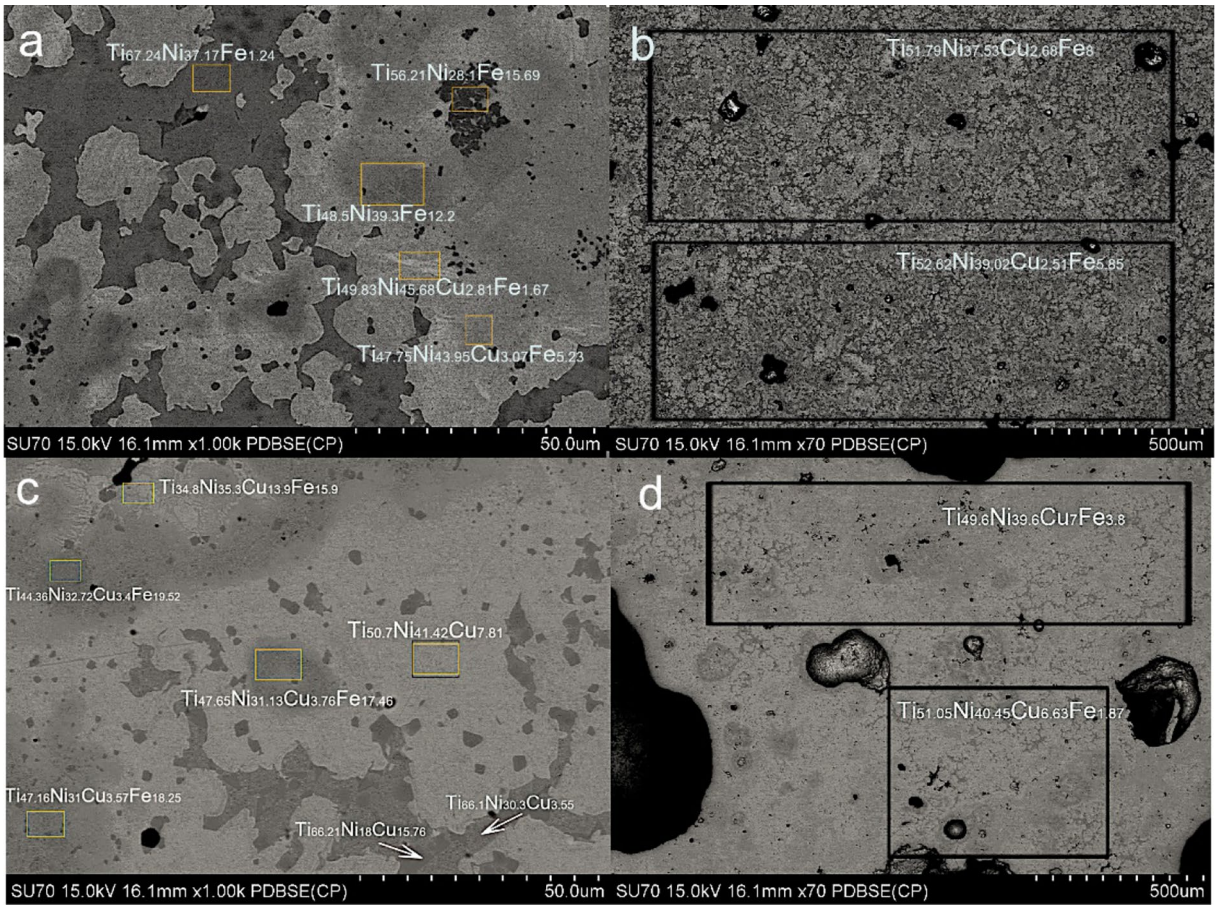


**Fig. 6** SEM-BSE Micrograph (wt. embedded EDS results) of **a**–**b** Cu2.5 (D2) and **c**–**d** Cu7.5 (D4)

**Table 4** Transformation temperatures for different samples are extracted from the references

| For Fe-based $Ni_{100-x}Ti_{50}Fe_x$ (at.%) x: | B19'->R (As) | R->B2 (As') | B2->R (Ms') | R->B19' (Ms) |
|---|---|---|---|---|
| 2.5 [22] | −9 | 23 | 14 | −27 |
| 3 [21] | | | −65 | |
| 4 [22] | | | −57 | X |
| 4 [3] | | | ~ −31 | |
| 10 [3] | None | None | None | None |
| For Cu-based NiTi $Ni_{100-x}Ti_{50}Cu_x$ (at.%) x: | B19->B2 | B19'->B19 | B2->B19 | B2->B19' (B19->B19') |
| 5 [2] | 38 | – | – | 36 |
| 7.5 [2] | 32 | −37 | 24 | 17 |
| 10 [2] | 42 | −81 | 40 | 19 |
| 7 [4] | ~52 | | ~47 | |

of the reaction. The fundamental reason for the changes observed in the variation of the transformation temperature results is the mixture enthalpy, as evidenced by both thermodynamic analyses, XRD and SEM analysis. In previous research, particularly with high-entropy alloys, efforts were made to achieve homogeneity in powder mixtures, and similar results were obtained despite heat treatment [14–16, 28]. In other words, compounds with low and high mixture enthalpies tend to segregate from each other.

According to DSC analysis, samples containing 7.5 at.% Fe exhibited a second martensitic phase. It was apparent that Cu was the dominant element in the B2 crystal structure.

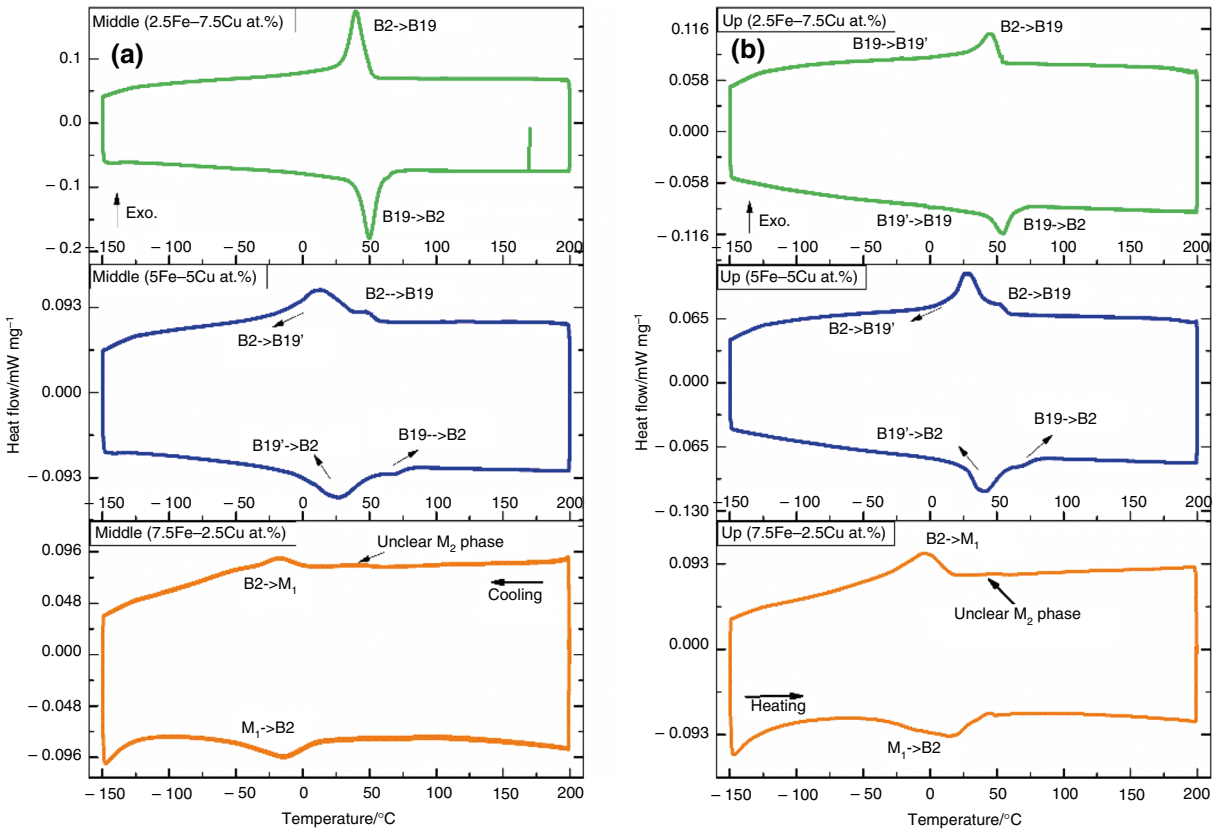


**Fig. 7** DSC graph of **a** middle and **b** upper part of the samples

For instance, the emergence of the R-phase martensite with Fe is known, but it has been reported that martensitic transformation is entirely suppressed at Fe contents exceeding 6 at.% [3, 21, 22]. In this study, however, even at 7.5 at.% Fe, an ambiguous second martensitic phase alongside the B19' phase was observed at Ap (−14.74 °C) and Mp (−16.34 °C), respectively (for mid. part). Moreover, the Cu content in the structure was only 2.5 at.%. Sample Cu2.5 exhibited a significant deviation in Ap-Mp values between the upper (1.6 °C) and middle (18.6 °C) portions, indicating clear separation of Fe from Cu in the system, and leading to the formation of precipitates. Consequently, the Fe content within the B2 phase decreased. The lowest Ap-Mp and Af-Ms difference was observed in the Cu7.5 sample (middle: 8, upper: 9 °C for Af-Ms). This suggested that as the Fe content decreased, segregations in the system decreased. Metallographic examination supported inconsistencies in elemental distribution with increasing iron content, as well as the large FWHM value in DSC, supporting this observation. The reason could be the separation of initially formed intermetallics ($Fe_xTi_y$) in the first region heated by the ignition wire and initiated melting at a high temperature, due to the low enthalpy value of the intermetallics and the positive enthalpy interactions of copper with other elements. When examining the maximum

**Table 5** The transformation temperature of the samples

| Samples Ti:50, Ni:40 (at.%) | As | Af | Ms | Mf | Af-Ms | Mp | Ap | Ap-Mp | Transf Enth.of Mart / (mJ $mg^{-1}$) | FWHM |
|---|---|---|---|---|---|---|---|---|---|---|
| Cu2.5 (mid.) | −65* | 12 | 2 | −41.8* | 10 | −16,3 | −14,7 | 1.6 | 1.62 | 22.22 |
| Cu5 (mid.) | −2 | 62 | 46.9 | −18.6 | 15 | 13.26 | 27.06 | 13.8 | 9.66 | 39.7 |
| Cu7.5 (mid.) | 39.75 | 60 | 52 | 28.5 | 8 | 39,65 | 49,96 | 10,3 | 11.04 | 11.8 |
| Cu2.5 (up.) | −43* | 40 | 18 | −47* | 22 | −4.2 | 14,06 | 18,59 | 5.82 | 31.4 |
| Cu5 (up.) | 25.5 | 78 | 59 | 13 | 19 | 27.21 | 41.43 | 14.22 | 7.68 | 19.4 |
| Cu7.5 (up.) | 44 | 67 | 58 | 32 | 9 | 44,24 | 54,74 | 10,49 | 6.72 | 17.7 |

reached temperatures, it was seen that 7.5 at.% Fe is higher than 2.5 at.% Fe. It is likely that during slow cooling inside the furnace after the reaction, liquid inter-dendritic regions might have resulted in the formation of Fe-rich areas and accentuated grain structure. The presence of inter-dendritic intermediate phases composed of TiFe and $Ni_{25}Ti_{50}Fe_{25}$, as indicated by XRD analysis, corroborated this. Zhang et al. noted that homogenization sharpens the peaks. The Cu7.5 sample might confirm this [29]. The Ap and Mp values for the portions taken from the middle and upper parts of this sample were close to each other. Similarly, their FWHM values were close, while they were half of those from the Cu2.5 sample (see Table 5).

## Conclusions

It was successfully produced with SHS by adding Fe and Cu to NiTi in varying proportions. Accordingly, the following results have been reached.

(1) Among the samples produced with SHS at a preheating temperature of 230/240 °C, the high Cu ratio sample $Ti_{50}Ni_{40}Fe_{2.5}Cu_{7.5}$(D1) experienced interrupted propagation. As explained in the results, the increase in copper ratio caused a decrease in the maximum combusting temperature, which was necessary for the propagation of the reaction. Increasing the Fe content up to 5 at.% facilitated propagation. The reason for this was that, while Cu-related alloys reacted with an endothermic enthalpy, Ni–Ti and Ti–Fe caused an exothermic mixing enthalpy due to the formation of intermetallic compounds.

(2) Two different samples were taken from the middle and upper part of the specimen for DSC analysis because elemental distribution was not found homogenous and observed TiFe–NiTiFe phases in the both SEM–EDS and XRD analysis. Additionally, an increase in Fe resulted in a more inter-dendritic structure, as found in the SEM–EDS analysis. The reason behind this is the precipitation of Fe as an intermetallic phase, and its inability to homogeneously enter the B2 structure with Cu due to the positive mixing enthalpy of the Cu with the other elements. It proves that method of SHS is not the main reason of the homogeneity. It is also a results of the mixing enthalpies of the alloys.

(3) Cu played a more dominant role than Fe in controlling transformation temperatures and the type of martensite structure. Increasing the copper while decreasing Fe content led to higher transformation temperatures. The hysteresis of martensitic transformation (Af-Ms) and Ap-Mp was tended to decrease, except for Cu2.5 (mid. section), which did not conform to this trend. This deviation was attributed to the heterogeneity caused by the high Fe content.

(4) The difference between Ap and Mp in sample no D4 compared to other samples was quite small, thus it was the most homogeneous structure. The martensitic hysteresis curve of Cu7.5 was 8 and 9 °C for the middle and upper parts, respectively. In Cu5, the B19- > B19' transformation was absent, but simultaneous B2- > B19' and B2- > B19 transformations were observed in both the middle and upper sections.

**Acknowledgements** The authors would like to express their gratitude to Dr. Paola Bassani (CNR ICMATE, Italy) for her invaluable assistance in the characterization process.

**Author contributions** Berk Keskin proposed methodology, conceptualization, investigation, and writing—original Draft. Bora Derin performed supervision, methodology, writing—review, and validation.

## Declarations

**Conflict of interest** The corresponding author declares that they have no conflict of interest.

## References

1. Jani JM, Leary M, Subic A, Gibson MA. A review of shape memory alloy research, applications and opportunities. Mater Des. 2014;56:1078–113.
2. Nam TH, et al. Cu-content dependence of shape memory characteristics in Ti–Ni–Cu alloys. Mater Trans, JIM. 1990;31:959–67.
3. Choi M-S, Ogawa J, Fukuda T, Kakeshita T. Stability of the B2-type structure and R-phase transformation behavior of Fe or Co doped Ti–Ni alloys. Mater Sci Eng A. 2006;438–440:527–30.
4. Nespoli A, Villa E, Besseghini S. Characterization of the martensitic transformation in Ni50−xTi50Cux alloys through pure thermal measurements. J Alloys Compd. 2011;509:644–7.
5. Otsuka K, Ren X. Physical metallurgy of Ti–Ni-based shape memory alloys. Prog Mater Sci. 2005;50:511–678.
6. Nam TH, et al. Shape memory characteristics and lattice deformation in Ti–Ni–Cu alloys. Mater Trans, JIM. 1990;31:1050–6.
7. Li J, Wang H, Liu J, Ruan J. Effects of Nb addition on microstructure and mechanical properties of TiNiNb alloys fabricated by elemental powder sintering. Mater Sci Eng A. 2014;609:235–40.
8. Lo Y, Wu S, Horng H. A study of B2↔ B19↔ B19′ two-stage martensitic transformation in a Ti 50 Ni 40 Cu 10 alloy. Acta Metall Mater. 1993;41:747–59.
9. Goryczka T, Van Humbeeck J. NiTiCu shape memory alloy produced by powder technology. J Alloys Compd. 2008;456:194–200.
10. Tong Y, et al. Novel TiNiCuNb shape memory alloys with excellent thermal cycling stability. J Alloys Compd. 2019;782:343–7.
11. Lai HM, Liu FS. Influence of Nb addition on phase transformation of TiNiFe shape memory alloy. Mater Sci Forum. 2011;687:494–9.
12. Chluba C, et al. Ultra-low fatigue quaternary TiNi-based films for elastocaloric cooling. Shape Mem Superelasticity. 2016;2:95–103.
13. Nayan N, et al. High-temperature deformation processing map approach for obtaining the desired microstructure in a

multi-component (Ni–Ti–Cu–Fe) alloy. Metall Mater Trans A. 2015;46:2201–15.
14. Sekhar RA, Nayan N, Bakshi SR. Microstructure and mechanical properties of NiTiCuFe multi-component alloy. Trans Indian Inst Met. 2018;71:2789–93.
15. Zhang Y, et al. Solid-solution phase formation rules for multi-component alloys. Adv Eng Mater. 2008;10:534–8.
16. Yang X, Zhang Y. Prediction of high-entropy stabilized solid-solution in multi-component alloys. Mater Chem Phys. 2012;132:233–8.
17. Singh AK, Kumar N, Dwivedi A, Subramaniam A. A geometrical parameter for the formation of disordered solid solutions in multi-component alloys. Intermetallics. 2014;53:112–9.
18. Takeuchi A, Inoue A. Classification of bulk metallic glasses by atomic size difference, heat of mixing and period of constituent elements and its application to characterization of the main alloying element. Mater Trans. 2005;46:2817–29.
19. Miedema A, De Boer F, Boom R. Model predictions for the enthalpy of formation of transition metal alloys. Calphad. 1977;1:341–59.
20. Li B, Rong LJ, Li Y-Y, Gjunter V. Synthesis of porous Ni–Ti shape-memory alloys by self-propagating high-temperature synthesis: reaction mechanism and anisotropy in pore structure. Acta Mater. 2000;48:3895–904.
21. Yi HC, Moore JJ. The combustion synthesis of Ni–Ti shape memory alloys. JOM. 1990;42:31–5.
22. Nishida M, Honma T. Phase transformations in Ti50Ni50-xFex alloys. J Phys Colloq. 1982;43:C4-225-C4-230.
23. Valeanu M, et al. Martensitic transformation of Ti50Ni30Cu20 alloy prepared by powder metallurgy. J Alloys Compd. 2011;509:4495–8.
24. Wu SL, et al. Phase transformation behavior of porous NiTi alloys fabricated by capsule-free hot isostatic pressing. J Alloys Compd. 2008;449:139–43.
25. Cheng GP, Xie ZL. Some results on shape memory properties of Ti50Ni25Cu25 melt-spun ribbons. J Alloys Compd. 2005;396:128–32.
26. Zhang Y-Q, et al. Influence of Fe addition on phase transformation behavior of NiTi shape memory alloy. Trans Nonferrous Met Soc China. 2017;27:1580–7.
27. Frenzel J, et al. Influence of Ni on martensitic phase transformations in NiTi shape memory alloys. Acta Mater. 2010;58:3444–58.
28. Hua X-J, et al. Development and property tuning of refractory high-entropy alloys: a review. Acta Metall Sin (Engl Lett). 2022;35:1231–65.
29. Zhang Z, Frenzel J, Neuking K, Eggeler G. Vacuum induction melting of ternary NiTiX (X= Cu, Fe, Hf, Zr) shape memory alloys using graphite crucibles. Mater Trans. 2006;47:661–9.